# Mechanical Loss in Multiferroic Materials at High Frequencies: Friction and the Evolution of Ferroelastic Microstructures

*Z. Zhao, X. Ding,* T. Lookman, J. Sun, and E. K. H. Salje**

The development of novel multiferroic device materials hits a fundamental limitation when the driving frequency is increased beyond 50 MHz. Ultimately, we want to use detectors, memory chips and converters between electric and magnetic signals at such high frequencies. The idea is, hence, that device materials need to be defect free because any extrinsic defect relaxation will be slower than the operating frequency and will hence absorb the external signal.[1–5] The solution of this conundrum was to use very clean multiferroic materials where the desired change of electric and magnetic dipoles is very fast in thin films. We will show in this paper that this solution does not work in most materials where coupling to ferroelasticity is strong. Empirically, it is already known that the movement of ferroelastic domain boundaries involves high losses and is highly dissipative (e.g. in relaxor materials).[6,7] However, the origin of these losses was unclear. In this paper we demonstrate that only two mechanisms dominate the loss effects, namely, the propagation of needle domains and the movements of wall kinks.

Dynamical shear applied to multiferroic materials with strong elastic strain interactions generates ferroelastic hysteresis loops related to domain rearrangements and subsequent changes of the associated parameters such as ferroelectricity, piezoelectricity and conductivity of the sample.[8–18] Its origin at low frequencies is the slow, athermal relaxations of twin patterns which can often be observed optically.[9,12] At high frequencies we expect that this is no longer the case, the changes due to confinement of strains is faster than the time needed to relax the domain pattern. The best way to observe the loss at moderately high frequencies is Resonance Ultrasonic Spectroscopy, RUS, where a small elastic strain ($10^{-7}$ ~ $10^{-5}$) is applied at frequencies near 1–10 MHz. In defect free materials without any twin microstructure the elastic RUS response has low losses.[17,18] Where microstructures occur, the signals show losses which are often very different from losses in low frequency experiments (different activation energies, different amplitudes, etc). It has therefore been concluded that the relevant relaxation pathways are strongly frequency dependent even in the $10^{-3}$ ~ $10^{7}$ Hz regime[17,18] and it is expected that such dispersion is also extrapolated to higher frequencies. The key question then is: what mechanisms are responsible for the observed energy absorption?

This question is of fundamental importance because multiferroic displacive systems can be imagined to relax at phonon time scales and dissipation should occur only when the time scale of the exciting strain approaches $10^{12}$ Hz. The observed low frequency absorption is hence usually explained by extrinsic defects which pin and de-pin microstructures and hence dramatically reduce the time window for dissipation. The observation of dissipation and absorption is often seen as 'proof' for the existence of extrinsic defects which interact with the microstructure.[8,10,19,20] It also offers a possibility to analyze the internal structure of the twin boundaries (such as its conductivity, ferroelasticity and ferromagnetism) via their interaction with suitable extrinsic defects.[14,21]

While this approach offers exciting new opportunities to generate novel functional interfaces and to characterize them through their interaction with known defects, we will show in this paper that intrinsic pinning centers also exist in complex multiferroic materials. The dynamic behavior has hence an extrinsic defect component and some 'background' dynamics which is dominated by jamming and avalanches (~jerks) of the intrinsic microstructure.[22,23] No extrinsic defects are required for the background absorption so that future experimental work needs to carefully separate these two features, namely the intrinsic jamming and the extrinsic defect pinning.

The reason for intrinsic pinning (~jamming) lies in the complexity of microstructures which depend sensitively on their history: e.g., thermal quench and low temperature shear deformation lead to fundamentally different types of mesoscopic microstructures and the simplest element of all patterns remains the local twin boundary.[9,24,25] The complexity of the pattern originates from the bending, interpenetration, and formation of superstructures such as needle domains and tweed patterns. Such complex patterns can be characterized by the number of junctions between twin walls, the density of needle domains, and the penetration angle of twin boundaries through the sample surface. We now show that the dominant geometrical movement at all frequencies is the progression and retraction of needle domains and the sideways movement of twin walls and their absorption mechanism. For this we use a model

Dr. Z. Zhao, Dr. X. Ding, Prof. J. Sun, Prof. E. K. H. Salje
State Key Laboratory for Mechanical Behavior of Materials
Xi'an Jiaotong University
Xi'an 710049, China
E-mail: dingxd@mail.xjtu.edu.cn; ekhard@esc.cam.ac.uk
Prof. E. K. H. Salje
Department of Earth Sciences
University of Cambridge
Cambridge CB2 3EQ, UK
Dr. X. Ding, Dr. T. Lookman, Prof. E. K. H. Salje
Theoretical Division and Center for Nonlinear Studies
Los Alamos National Laboratory
Los Alamos, NM 87545, USA

DOI:10. 1002/adma.201300655

which describes the displacive collapse of a sheared ferroelastic structure.[23]

Our model is constructed to be generic for all ferroelastic phase transitions by choosing as 'order parameter' the shear angle which leads to ferroelastic twinning. This twinning and the mobility of the twin walls defines ferroelasticity.[8] Comparing this configuration with the ferroelastic transition from cubic to tetragonal in $SrTiO_3$ at 105 K, we focus on the modeling of a plane perpendicular to the twin plane (i.e. our axes are [101] and [$\bar{1}$01] in the Pm $\bar{3}$m setting). Equivalent planes can be found in all ferroelastic systems. The simulations were conducted with three interactions in a monoatomic, two-dimensional lattice. The Landau potential of such materials is implemented in the model by using anharmonic springs which mimic the potential; three springs are necessary, namely two harmonic springs along the main axes and one diagonal Landau spring which gives the landau potential as a function of its elongation and hence of the local shear of the sample. The three interactions are: (1) harmonic nearest neighbor interactions (elastic springs), $U(r) = K1(r-1)^2$, black in Figure S1; (2) double well potentials between next nearest neighbors, $U(r) = -10(r-\sqrt{2})^2 + 2000(r-\sqrt{2})^4$; diagonals in the square lattice, red springs online in Figure S1; (3) fourth order interactions (springs) between the third nearest neighbors which are parallel to the nearest neighbor interactions with $U(r) = -(r-2)^4$ and long green lines in Figure S1. r is the distance vector with lattice repetition unit 1. The resulting potential is a sum of the three interactions (further details with all parameters in Table S1).

We use the potential to simulate the shear instability in a sandwich configuration with two horizontal domain boundaries (**Figure 1**a). The calculated cell contains two buffer layers at the top and bottom of the two dimensional sheet. These buffer layers were sheared by the external boundary conditions (fixed external strain, hard boundary conditions). Free boundary conditions are adopted to enable needle domains to nucleate from the free surface. The computer code LAMMPS was used with an NVT ensemble and the temperature of the sample was held constant by the Nosé-Hoover thermostat.

The second nearest neighbor interactions were adjusted to yield a ground state with a sheared lattice (shear angles ± 4°). The external shear at the upper and lower buffer layers of the sample stabilizes one domain orientation (+4°) and destabilizes the other (–4°). Upon loading, the increasing strain is initially compensated by an elastic deformation until a threshold is reached where the unstable domain decomposes into a multitude of twinned micro domains.[23] Inside domain walls we find the spontaneous nucleation of kinks and their movement under external shear strain. These complex patterns contain most of the important dynamical features moving needle domains and kinks (Figure 1). During the simulations, unlike Ref. [23] where the shear strain increased linearly with time, we choose here an oscillatory time dependence for the shear strain $e = e_o + \Delta e$, where $\Delta e = A \sin(\omega t)$, which mimics the frequency dependence of RUS experiments. The temperature for the simulation of a kink movement was set to be $0.1T_{VF}$. Here and elsewhere, $T_{VF}$ refers to the Vogel-Fulcher temperature. This temperature limits the thermally excited kink movement to the a-thermal regime. Our simulations are hence essentially

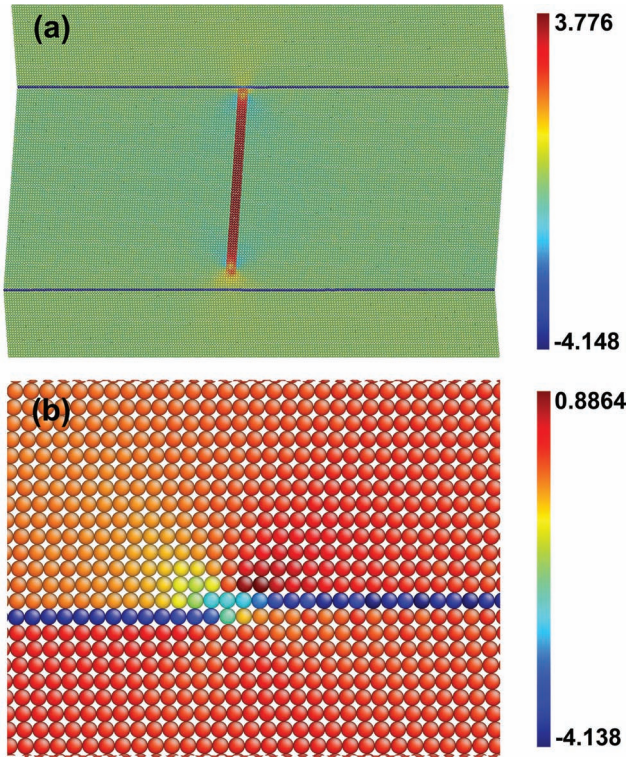


**Figure 1.** Sheared unit cell of the driven system.[23] (a) The single needle domain (red) connects the two horizontal twin boundaries (blue) at the initial stage and then retracts from the lower twin boundary. (b) The kink is seen at the single blue domain wall. It moves to the left under applied external strain. The color scheme represents the local shear angle from the underlying bulk structure ($|\Theta_{vertical}| - 4° + \Theta_{horizontal}$), for details see Ref. [23]

a-thermal so that thermal excitations are irrelevant for the analysis. As in Ref. [23], at low temperatures we find power law distributions for the energy of avalanches but at high temperatures, when the sample is still ferroelastic but approaches the melting point, we find thermally excited Vogel-Fulcher distributions. Thus, $T_{VF}$, defines the cross-over temperature between the Vogel-Fulcher regime and the power-law regime. The statistical collective behavior of a twin pattern at this temperature is described by a power law probability P(J) of pinning and depinning events J: $P(J) \sim J^{-\varepsilon}$.[26] The MD temperature for the needle domain movement was $T_{VF}$.

The dynamics of a single needle domain is as follows. After the first five cycles to consolidate the microstructure, we find that the needle domain is disconnected from the horizontal twin boundary at least during parts of the driving cycle (Figure 1a). This situation is characteristic for metastable domain structures before they are subjected to further strain. We set the external strain $e_o$ to the de-pinning point where the needle just detaches itself from the horizontal twin boundary in Figure 1. Increasing the strain (increasing e via $\Delta e$) will then stabilize the domain pattern, whereas reducing e during the negative half period of the sine-wave destabilizes the needle domain and ruptures the junction between the needle twin and the horizontal twin boundary. After rupture, the needle domain is free of the twin wall and can retract and ultimately progress when the strain

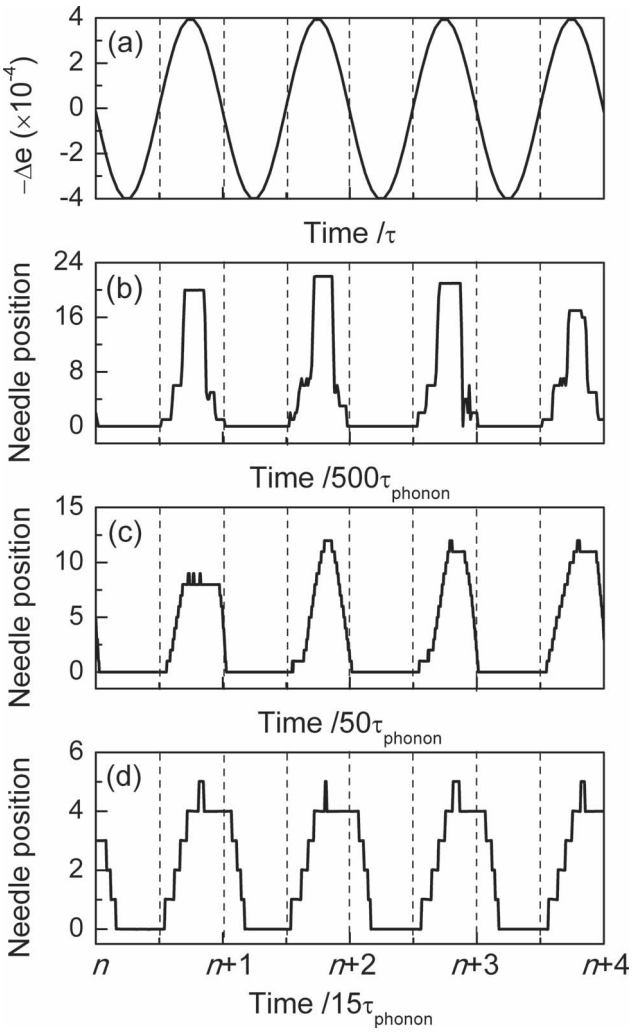


**Figure 2.** Position of the needle tip compared with the driving strain oscillation ($\Delta e = A \sin(\omega t)$). $\tau$ is the time period of input sine-wave and $\tau_{phonon}$ is the time period of phonon. Note the increasing width of the profile when the frequency is increased. The onset of the domain retraction is retarded with respect to the reflection points of the driving force while the progression of the needle starts later than the reversed driving strain ($\Delta e$). The profiles are non-symmetric with slow retraction and faster progression.

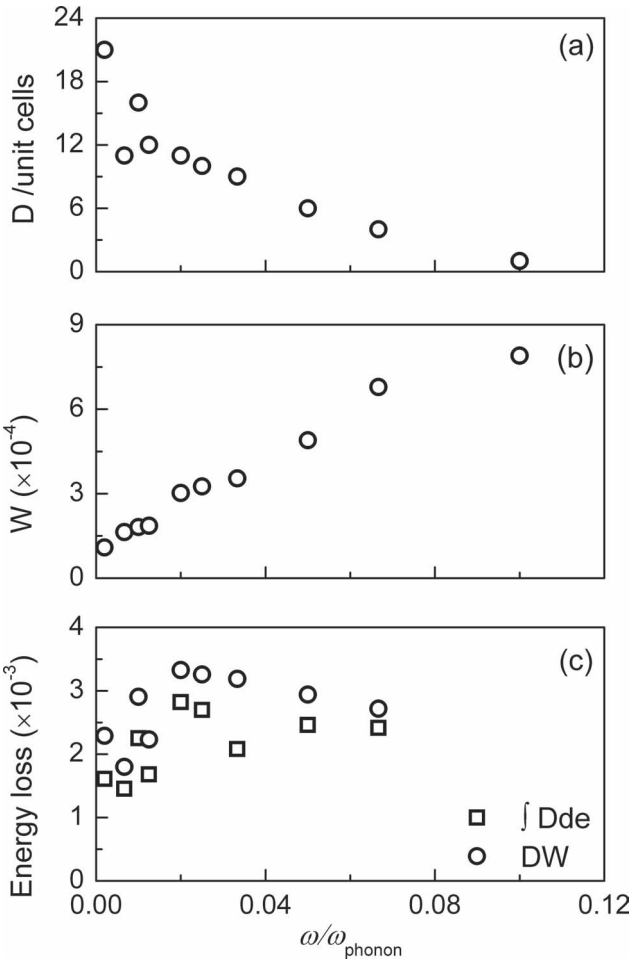


**Figure 3.** Frequency dependence of the gap, D, between the needle tip and the orthogonal twin boundary, the width of the strain hysteresis, W, and the product DW (circle symbols) (also evaluated as an integral over the strain hysteresis (square symbols)). This figure shows that although the gap (D) and the width of the strain hysteresis (W) are a function of frequency, the energy loss by the pinning/de-pinning of needles is (almost) independent of frequency.

increases again. A representative sequence of such oscillations is shown in **Figure 2**. We repeated these forcing experiments over several cycles and over a large frequency range between $\omega = \omega_{phonon}/10$ and $\omega = \omega_{phonon}/500$ (where $\omega_{phonon}$ is the phonon frequency). The results in Figure 2 demonstrate that the phase angle between the exciting wave and the tip position is large and changes with frequency. This was previously measured but not explained in RUS experiments.[18,22]

**Figure 3**a shows that the amplitude of the 'free' movement of the needle, D = maximum distance between the needle tip and the pinning horizontal twin wall, decreases with increasing frequency while the width of the ferroelastic hysteresis (W) increases (Figure 3b). The width (W) is fairly well defined with small thermal fluctuations at high frequencies. This is not the case for the amplitude (D) at low frequencies (Figure 2b and 3a). Here we find fluctuations of some 30% when the shear excitation is continued over several periods. Fluctuations decrease when the frequency increases (Figure 2c and 2d) because now the time scale for the propagation is set by the time scale of the exciting shear wave and not by the thermal fluctuations during the needle propagation. Figure 3 contains the integrated hysteresis ($\int D\,de$) which shows large fluctuations at low frequencies. The hysteretic integral can also be estimated from the product DW. Both data sets are plotted as function of frequency in Figure 3c and show that the energy loss is (almost) independent of frequency.

We now focus on the second excitation, namely, the movement of kinks as a result of applied shear strain beyond the yield point or plastic flow regime.[23] In complex patterns, kinks typically nucleate near junctions between twin walls or at the intersection of a twin wall with a surface. Under strain they move inside the twin wall to increase the stable domain state and reduce the unstable state. The kinks move with a constant

velocity, and its speed is reduced drastically by collision with obstacles, which can lead to a complete pinning of the kinks in extreme cases. When loading, the typical obstacles are junctions between twins (Figure S2(a)). When the kink approaches a junction, some pinning occurs so that the kink is first attracted and then retarded (Figure S2(b)). The initial free movement of the kink reemerges when the pinning force is overcome by larger strain fields. When the strain is reduced we find that the kink movement does not immediately reverse its direction but that the junctions (and the vertical twins) are destabilized and disappear first. This sequence of nucleation of kinks and the subsequent destruction of the nucleation center and dissipation makes the movement of kinks irreversible even for small amplitudes.

The second movement occurs when the nucleation center of kink has disappeared: in this case the kink can oscillate when the accumulated oscillation strain $\int \Delta edt$ is a sine-wave (**Figure 4**a). The strain oscillation is asymmetric with respect to the zero stress and one finds that kink movements are not balanced between the right and left direction. This often leads to the disappearance of the kink at the surface and hence the topological destruction of the kink. The only condition to maintain the kink in the same twin wall is to have a strictly symmetrical excitation so that the kink oscillates around its zero stress position. We changed the frequency of the exciting strain field in this situation and measured the oscillatory kink position. The correlation between the accumulated oscillation strain $\int \Delta edt$ and the kink positions is shown in Figure 4. The free movement of the kink occurs almost at a constant speed. Only when the direction of the movement is inverted do we obtain accelerated movement and a frequency dependence of the response function (Figure 4b–d). The constant speed of the kink in the defect free case stems from phonon scattering visible in Figure 1b as localized dynamic lattice distortions following the moving kink. This effect is akin to propagating acoustic phonons which transfer the friction loss into the bulk (and resemble somewhat Cherenkov radiation in the case of fast injected particles which travel faster than the speed of light). This phonon drag prevents the accelerated movement of the kink. If the driving is stronger than that required for the movement, the surplus energy is absorbed by the phonons with no visible effect on the kink movement.

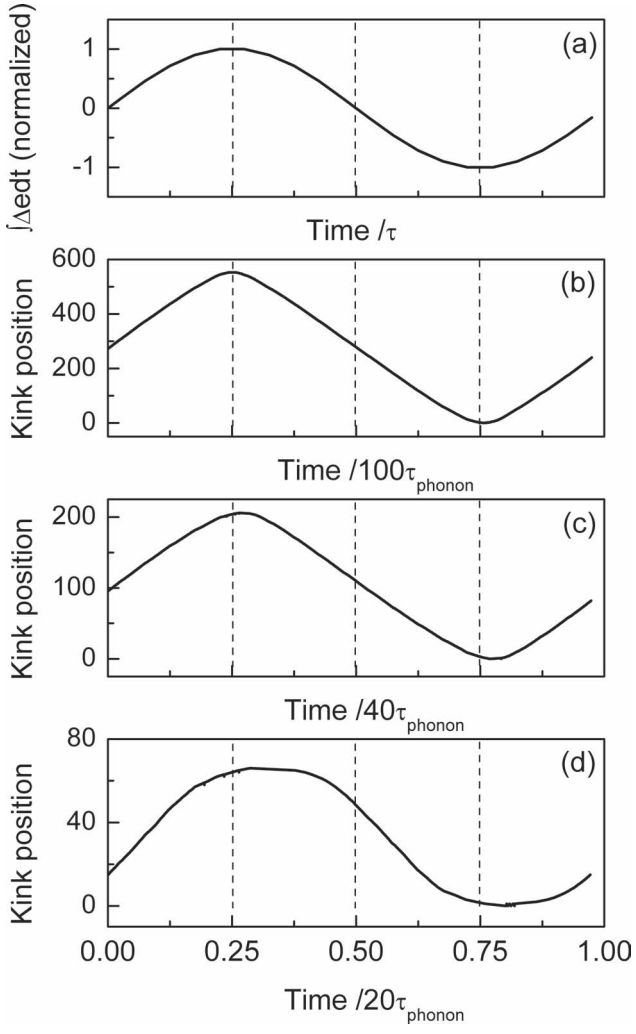


**Figure 4.** Time evolution of the kink position under strain forcing for three different frequencies of the applied strain field. $\int \Delta edt$ is the accumulated oscillation strain; $\tau$ is the time period of input sine-wave and $\tau_{phonon}$ is the time period of phonon. The kink propagation is in phase with the strain for low frequencies but displays retardation and phase shifts at high frequencies.

Our results clearly demonstrate that multiferroic device materials will always encounter energy loss due to changes of their microstructure. This loss does not require the involvement of defects. The main loss mechanisms are summarized below.

1. Moving domain patterns show pinning and depinning behavior near junctions between twin boundaries along different directions, and the surface. No extrinsic defects are required in this mechanism. Each event leads to a sudden energy increase (jerk) which was observed experimentally[27,28] and predicted analytically by statistical models.[26] The jerk statistics were simulated in Ref. [23] but the actual physical events which provoke the jerk were previously unknown.
2. Damping, friction and absorption of domain wall movements are only partly related to the 'free' movement but are dominated by the pinning/de-pinning behavior. There is additional friction during the subsequent movement of the needle when retraction changes to propagation (below the reversibility point). Both effects combine to make the needle movement 'lossy' and change the retardation between the applied strain and the needle position. This change of phase angle was observed experimentally.[22]
3. Kink propagation is lossy because of the nucleation and pinning near junctions. This also leads to retardation of the response relative to the exciting force.[22] The free kink absorbs less energy but advances with constant frequency. Any surplus energy is then absorbed and increases the temperature of the sample. This broad background excitation leads to Fano-type profilesi nR USs tudies.

Devices materials cannot avoid these intrinsic absorption mechanisms other than by operating at sufficiently low strains and temperatures to avoid de-pinning or by de-twinning the material. Additional extrinsic pinning by defects can help to pin the microstructure (if de-twinning proves impossible) but

only if the defects do not relax and absorb strain energy by themselves.

In summary, energy absorption in multiferroic materials stems typically from strain relaxation which can be strong even when no extrinsic defects exist in the material. Our computer simulations of a simple two-dimensional model on a generic, proper ferroelastic material have identified the dissipative mechanisms associated with the dynamical motion as 1.) Advance and retraction of needle-shaped twin domains and, 2.) Movement of kinks inside twin boundaries. Both movements involve friction losses. The friction loss in needle movements is almost frequency independent. The loss occurs mainly during the pinning and de-pinning of the needle at another twin wall. The dynamical response involves a retardation of the needle movement relative to the applied force. This phase angle is strongly frequency dependent, as observed experimentally in Resonance Ultrasonic Spectroscopy. Freely traveling kinks propagate with a constant speed, any higher forcing leads to stronger phonon scattering but does not increase the speed. No defects are involved in these mechanisms.

## Supporting Information

Supporting Information is available from the Wiley Online Library or from the author.

## Acknowledgements

We appreciate the support of NSFC (51171140, 51231008), the 973 Program of China (2010CB631003, 2012CB619402) and 111 project (B06025). EKHS is grateful for support by the Leverhulme fund (RG66640) and EPSRC (EP/K009702/1).

Received: February 7, 2013
Published online: May 6, 2013

[1] B. Coluzzi, A. Biscarini, G. Mazzolai, F. M. Mazzolai, A Tuissi, F. Agresti, S. Lo Russo, A. Maddalena, P. Palade, G. Principi, *J. Alloys Compd.* **2008**, *456*, 118–124.
[2] S. J. Doo, R. Thomas, R. S. Katiyar, J. F. Scott, H. Kohlstedt, A. Petraru, S. H. Cheol, *Rep. Prog. Phys* **2012**, *75*, 076502.
[3] M. Correa, A. Kumar, S. Priya, R. S. Katiyar, J. F. Scott, *Phys. Rev. B* **2011**, *83*, 014302.
[4] W. Eerenstein, N. D. Mathur, J. F. Scott, *Nature* **2006**, *442*, 759–765.
[5] J. F. Scott, *Nature Materials* **2007**, *6*, 256–257.
[6] M. A. Carpenter, J. F. J. Bryson, G. Catalan, S. J. Zhang, N. J. Donnelly, *J. Phys.: Condens. Matter* **2012**, *24*, 045902.
[7] G. Catalan, J. Seidel, R. Ramesh, J. F. Scott, *Rev. Mod. Phys.* **2012**, *84*, 119–156.
[8] E. K. H. Salje, *Annu. Rev. Mater. Res.* **2012**, *42*, 265–283.
[9] a) M. T. Bryan, J. Dean, D. A. Allwood, *Phys. Rev. B* **2012**, *85*, 144411. b) R. J. Harrison, E. K. H Salje, *Appl. Phys. Lett.* **2010**, *97*, 021907.
[10] M. A. Carpenter, C. J. Howard, B. J. Kennedy, K. S. Knight, *Phys. Rev. B* **2005**, *72*, 024118.
[11] a) S. Wada, T. Tsurumi, *Br. Ceramic Trans.* **2004**, *103*, 93; b) R. J. Harrison, S. A. T. Redfern, E. K. H. Salje, *Phys. Rev. B* **2004**, *69*, 144101.
[12] a) P. Wu, X. Ma, Y. Li, V. Gopalan, L-Q. Chen, *Appl. Phys. Lett.* **2012**, *100*, 092905; b) Y. Gu, K. Rabe, E. Bousquet, V. Gopalan, L.-Q. Chen, *Phys. Rev. B* **2012**, *85*, 064117.
[13] Y. Ivry, D. Chu, J. F. Scott, E. K. H. Salje, C. Durkan, *Nano Lett.* **2011**, *11*, 4619–4625.
[14] M. A. Carpenter, E. K. H. Salje, *Eur. J. Mineral.* **1998**, *10*, 693–812.
[15] R. J. Hemley, J. Shu, M. A. Carpenter, J. Hu, H. K. Mao, K. J. Kingma, *Solid State Commun.* **2000**, *114*, 527–532.
[16] Y. Ivry, D. Chu, J. F. Scott, C. Durkan, *Adv. Funct. Mater.* **2011**, *21*, 1827–1832.
[17] M. A. Carpenter, E. K. H. Salje, C. J. Howard, *Rhys. Rev. B* **2012**, *85*, 224430.
[18] V. Stepkova, P. Marton, J. Hlinka, *J. Phys.: Condens. Matter* **2012**, *24*, 212201.
[19] G. Fan, Y. Zhou, K. Otsuka, X. Ren, K. Nakamura, T. Ohba, T. Suzuki, I. Yoshida, F. Yin, *Acta Mater.* **2006**, *54*, 5221–5229.
[20] D. Xue, Y. Zhou, X. Ding, K. Otsuka, J. Sun, X. Ren, *Acta. Mater.* **2011**, *59*, 4999–5011.
[21] a) E. K. H. Salje, *ChemPhysChem* **2010**, *11*, 940–950; b) E. A. Eliseev, A. N. Morozovska, Y. Gu, A. Y. Borisevich, L.-Q. Chen, V. Gopalan, S. V. Kalinin, *Phys. Rev. B* **2012**, *86*, 085416; c) S. Van Aert, S. Turner, R. Delville, D. Schryvers, G. Van Tendeloo, E. K. H. Salje, *Adv. Mater.* **2012**, *24*, 523–527.
[22] E. K. H. Salje, M. A. Carpenter, *Appl. Phys. Lett.* **2011**, *99*, 051907.
[23] E. K. H. Salje, X. Ding, Z. Zhao, T. Lookman, A. Saxena, *Phys. Rev. B* **2011**, *83*, 104109.
[24] X. Ding, Z. Zhao, T. Lookman, A. Saxena, E. K. H. Salje, *Adv. Mater.* **2012**, *24*, 5385–5389.
[25] E. K. H. Salje, X. Ding, Z. Zhao, T. Lookman, *Appl. Phys. Lett.* **2012**, *100*, 222905.
[26] K. A. Dahmen, Y. Ben-Zion, J. T. Uhl, *Nat. Phys.* **2011**, *7*, 554–557.
[27] E. K. H. Salje, J. Koppensteiner, M. Reinecker, W. Schranz, A. Planes, *Appl. Phys. Lett.* **2009**, *95*, 231908.
[28] M. C. Gallardo, J. Manchado, F. J. Romero, J. del Cerro, E. K. H. Salje, A. Planes, E. Vives, R. Romero, M. Stipcich, *Phys. Rev. B* **2010**, *81*, 174102.